

# pp Interaction at Very High Energies in Cosmic Ray Experiments

A. Kendi Kohara , Erasmo Ferreira and Takeshi Kodama  
*Instituto de Física, Universidade Federal do Rio de Janeiro,*  
*C.P. 68528, Rio de Janeiro 21945-970, RJ, Brazil*

An analysis of p-air cross section data from Extensive Air Shower (EAS) measurements is presented, based on an analytical representation of the pp scattering amplitudes that describes with high precision all available accelerator data at ISR, SPS and LHC energies. The theoretical basis of the representation, together with the very smooth energy dependence of parameters controlled by unitarity and dispersion relations, permits reliable extrapolation to high energy cosmic ray and asymptotic energy ranges. Calculations of  $\sigma_{p\text{-air}}^{\text{prod}}$  based on Glauber formalism are made using the input values of the quantities  $\sigma$ ,  $\rho$ ,  $B_I$  and  $B_R$  at high energies, with attention given to the independence of the slope parameters, with  $B_R \neq B_I$ . The influence of contributions of diffractive intermediate states, according to Good-Walker formalism, is examined. The comparison with cosmic ray data is very satisfactory in the whole pp energy interval from 1 to 100 TeV. High energy asymptotic behavior of cross sections is investigated in view of the geometric scaling property of the amplitudes. The observed energy dependence of the ratio between p-air and pp cross sections in the data is shown to be related to the nature of the pp cross section at high energies, that does not agree with the black disk image.

## I. INTRODUCTION

Recently detailed analyses of the experimental pp and p $\bar{p}$  scattering data have been performed for the highest energy domain available [1–3], with determination of amplitudes and cross sections based on the QCD stochastic vacuum model [4]. These analyses lead to very precise quantitative identification of analytic properties of the imaginary and real parts of the elastic scattering amplitudes, disentangling their presences in the observable quantities.

The amplitudes are founded on a QCD motivated model [5], controled by the unitarity and requirements from dispersion relations [6], thus furnishing a bridge between experimental data and microscopic models. It has also been shown that the high precision in the description of all available experimental data covering wide energy domain is attained with very smooth energy dependence [3]. We have then established a full  $(s, t)$  framework that allows safe interpolations and extrapolations required in the present era of expansion of the energy frontier. After successful reproduction of the data in the energy frontier of accelerator physics at the  $\sqrt{s} = 7$  TeV and 8 TeV energies of LHC, in the present work we direct our efforts to the examination of the cosmic ray data extracted from studies of Extensive Air Showers (EAS), where there is access to pp center of mass energies of up to 100 TeV. We feel that we start to approach the asymptotic regime where we hope to find the simplified dynamical description of elastic and diffractive processes in which the proton enters as a global object, determining the main features of the observables through its size and the modification of the QCD vacuum around it. In this high energy regime we may find the ideal conditions for the application of the concept and method of the Stochastic Vacuum Model [5] in which our amplitudes are based.

The purpose of the present work is to compare the proton-air production cross section, calculated in the framework of Glauber model using our representation of pp scattering as input, to the experimental values obtained from the available cosmic ray data. We are mainly concerned with the energies beyond the LHC experiments but also present results for EAS experiments in the region below 1 TeV.

We also study the behaviour expected for the p-air interaction at ultra-high energies, both as continuous extrapolation based on the region of the present data and as consequence of the known properties of the p amplitudes in  $b$ -space.

As mentioned above, our proton-proton scattering amplitudes have been carefully determined, permitting identification of the properties of the real part which is often neglected in calculations at high energies. We here stress again the importance of the difference between the slopes  $B_I$  and  $B_R$  of the imaginary and real parts. In the present work this detail enters in the application of Glauber formalism to evaluate the connection between p-air and pp cross sections.

Our analysis of energy dependence of amplitudes and observables in pp collisions shows that the total cross section has a neat  $\log^2 s$  form [3], as already indicated in several analyses [7]. An important feature of our results is that, the slope parameters, both for  $B_I$  and  $B_R$ , also a  $\log^2 s$  dependence. This is new and important finding. Generally accepted idea is that the slope of the differential cross sections varies like simple linear  $\log s$ , as in Regge phenomenology. Our new result has a crucial effect for the use of Glauber formalism in the analysis of p-air extended showers at the high energies of our concern, since the value of the slope  $B_I$ , together with the value of the total cross section, are the basic and strongly influent inputs of the calculation.

For the application of Glauber approach, we basically require information on the amplitudes in forward scattering. In our model these features are easily obtained taking small  $t$  limit [1, 2, 4] in our full- $|t|$  treatment. In these conditions the amplitudes take simpler exponential forms requiring only two parameters to specify each amplitude. The relevant parameters are then the total cross section  $\sigma$ , the ratio  $\rho$  between real and imaginary parts at  $t = 0$ , and the slopes  $B_I$  and  $B_R$  of each of the two parts. Our full- $t$  analysis [3] provides the energy dependence of these quantities with simple analytical forms that are appropriate for the whole energy range from 50 GeV to 100 TeV. With these forms at hand, we investigate the behaviour of quantities that are meaningful for the investigation of important features of the interaction in the forward region, and can make predictions for asymptotic energies.

The present paper is organized as follows. In the next section, we summarize our representation and the energy dependence of the necessary parameters for the application in calculation of p-air cross section in the Glauber formalism. We also show the high energy asymptotic behavior of quantities that have finite asymptotic limits, to obtain important information for extrapolation to the ultra-high energy and asymptotic domains. In Sec. IV we apply the results of the Glauber formalism to calculate p-air cross section using our inputs and compare with the experimental values. We show that the results for  $\sigma_{p\text{-air}}^{\text{prod}}(s)$  can be conveniently put in simple analytic form with very good accuracy, and then prove that the ratio  $\sigma_{p\text{-air}}^{\text{prod}}/\sigma_{pp}$  decreases slowly, approaching a finite limit at high energies. In Sec. V we discuss the geometric scaling property of our amplitude to understand the asymptotic behavior of p-air interaction and show how the non-black disk nature of our pp amplitude affects the asymptotic ratio of pA to pp cross sections. The last section is devoted to summary and discussion of the present work.

## II. FORWARD SCATTERING AMPLITUDES

In the treatment of elastic pp and p $\bar{p}$  scattering in the forward direction, with amplitudes approximated by pure exponential forms, the differential cross section is written

$$\frac{d\sigma}{dt} = \pi (\hbar c)^2 \left\{ \left[ \frac{\rho\sigma}{4\pi (\hbar c)^2} e^{B_R t/2} + F^C(t) \cos(\alpha\Phi) \right]^2 + \left[ \frac{\sigma}{4\pi (\hbar c)^2} e^{B_I t/2} + F^C(t) \sin(\alpha\Phi) \right]^2 \right\}, \quad (1)$$

where  $t \equiv -|t|$  and we must allow different values for the slopes  $B_I$  and  $B_R$  of the imaginary and real amplitudes. With  $\sigma$  in milibarns and  $|t|$  in  $\text{GeV}^2$ , we have  $(\hbar c)^2 = 0.3894$ . Since we work with  $B_R \neq B_I$ , treatment of the Coulomb interference requires a more general expression for the Coulomb phase, which has been developed before [1]. However, in the present work we only need the forward ( $|t| = 0$ ) nuclear amplitudes and slopes, and the Coulomb interaction does not enter, so that we put  $F^C(t) = 0$ .

The energy dependences of the four quantities are given by

$$\sigma(s) = 69.3286 + 12.6800 \log \sqrt{s} + 1.2273 \log^2 \sqrt{s}, \quad (2)$$

$$B_I(s) = 15.7848 + 1.75795 \log \sqrt{s} + 0.149067 \log^2 \sqrt{s}, \quad (3)$$

$$B_R(s) = 22.8365 + 2.86093 \log \sqrt{s} + 0.329886 \log^2 \sqrt{s}, \quad (4)$$

and

$$\rho(s) = \frac{3.528018 + 0.7856088 \log \sqrt{s}}{25.11358 + 4.59321 \log \sqrt{s} + 0.444594 \log^2 \sqrt{s}}, \quad (5)$$

where  $\sqrt{s}$  is in TeV,  $\sigma$  in milibarns,  $B_I$  and  $B_R$  are in  $\text{GeV}^{-2}$ ;  $\rho$  is dimensionless, passes through a maximum at about 1.8 TeV, and decreases at higher energies, with asymptotic value zero. The ratio  $B_R/B_I$  is always larger than one, as expected from dispersion relations [6], and behaves asymptotically like

$$\frac{B_R}{B_I} \rightarrow 1.80198 + \frac{4.82272}{\log \sqrt{s}} - \frac{118.192}{\log^2 \sqrt{s}}. \quad (6)$$

This ratio is not a monotonic function, having a small bump (it goes up to 1.86) at very large energies with  $\log \sqrt{s} \approx 30 - 40$ , and then decreases towards its asymptotic limit. The slopes and their ratio are shown in Fig. 1.

The dimensionless ratio

$$R_I = \frac{1}{(\hbar c)^2} \frac{\sigma}{16\pi B_I} \quad (7)$$

is often studied in considerations about the form of the pp interaction. The factor  $(\hbar c)^2$  is included to allow practical use of mixed units for  $\sigma$  (usually in milibarns) and  $B_I$  (usually in  $\text{GeV}^{-2}$ ). In our description of the pp system, as given by the energy dependences in Eqs. (2-5), this ratio has the high energy behaviour

$$R_I = \frac{1}{(\hbar c)^2} \frac{\sigma}{16\pi B_I} \rightarrow 0.341775 + \frac{1.50046}{\log \sqrt{s}} - \frac{30.2842}{\log^2 \sqrt{s}}. \quad (8)$$

This quantity is not monotonically varying, passing through a small bump in a range at very large energies, and then moving towards the asymptotic limit 0.342.

For amplitudes of pure exponential behaviour, as we have in this paper, this ratio is numerically equal to the ratio  $\sigma_{pp}^{\text{el},I}/\sigma$  between integrated elastic and total pp cross section. Thus this elastic ratio is also nearly 1/3, and the inelastic ratio is  $\sigma_{pp}^{\text{inel}}/\sigma \approx 2/3$ . We thus observe that the ratio is far from the value 1/2 that is characteristic of the idea of a black disk, where the interaction, considered as function of the impact parameter, is maximal inside a range  $b_0$  and zero outside this range. The conjecture of some authors is that at infinite energy the pp interaction could take the form of a black disk, as consequence of a kind of geometric scale property. Our results show that there is no such black disk behaviour. In our case, we observe an approximate geometrical scaling in the  $b$ -space differential cross

sections  $d^2\sigma^{\text{tot}}/d^2\vec{b}$  that start nearly constant (equal to 2), and then decrease in a scaled way, forming a diffused surface region. For the black disk instead the cross section behaves as the Heaviside step function. We show that the diffused range at high energies is responsible for the values of the ratios  $\sigma_{\text{pp}}^{\text{el,I}}/\sigma$  and  $\sigma_{\text{pp}}^{\text{inel}}/\sigma$  that are asymptotically different from 1/2. Details are presented and discussed in Sec. V.

We remark that we have used the slope  $B_I$  in the ratio (7) defined above. We may similarly define the ratio using the  $B_R$  slope, and then we obtain the high  $\sqrt{s}$  behaviour

$$R_R = \frac{1}{(\hbar c)^2} \frac{\sigma}{16\pi B_R} \rightarrow 0.1896 + \frac{0.325061}{\log \sqrt{s}} - \frac{5.23579}{\log^2 \sqrt{s}}. \quad (9)$$

With pure exponential form in the real amplitude, this fraction is equal to the ratio  $(\sigma_{\text{pp}}^{\text{el,R}}/\rho^2)/\sigma$ . Since  $\rho$  is small, the contribution of the real part to the integrated elastic cross section is also small.

The energy dependence of the two ratios  $R_I$  and  $R_R$  is shown in Fig. 2.

### III. GLAUBER CALCULATION

The information on the parameters given above for the pp interaction enters in the calculation of production cross section  $\sigma_{\text{p-air}}^{\text{prod}}$  that is obtained from the analysis of Extensive Air Showers.

Glauber method [8] provides the basic principles for the calculation of strong interactions with composite systems. The method first introduced in the treatment of scattering by deuterons was extended to more general nuclei, where the complexity of rescattering processes lead to considerations about the importance of intermediate diffracted states [9] not given as known external inputs. The application of the method to the analysis of proton-air collisions in the Extensive Air Showers (EAS) [10] gives the basic connection between the cosmic ray data and the hadronic scattering properties. As the basis of Glauber formalism is well known in its standard form, we present here the essential points giving the connection between pp and p-air processes, emphasizing the new features that arise from our treatment of pp amplitudes.

Our forward amplitudes  $(s, t)$  show different  $t$  behaviour in the imaginary and real parts, with different slopes  $B_I$  and  $B_R$ . Transferred to  $b$  space, we write amplitudes

$$\begin{aligned} \widehat{T}_{\text{pp}}(s, \vec{b}) &= \widehat{T}_R(s, \vec{b}) + i\widehat{T}_I(s, \vec{b}) \\ &= \frac{\sigma_{\text{pp}}^{\text{tot}}}{4\pi(\hbar c)^2} \left[ \frac{\rho}{B_R} e^{-\frac{b^2}{2B_R}} + i \frac{1}{B_I} e^{-\frac{b^2}{2B_I}} \right]. \end{aligned} \quad (10)$$

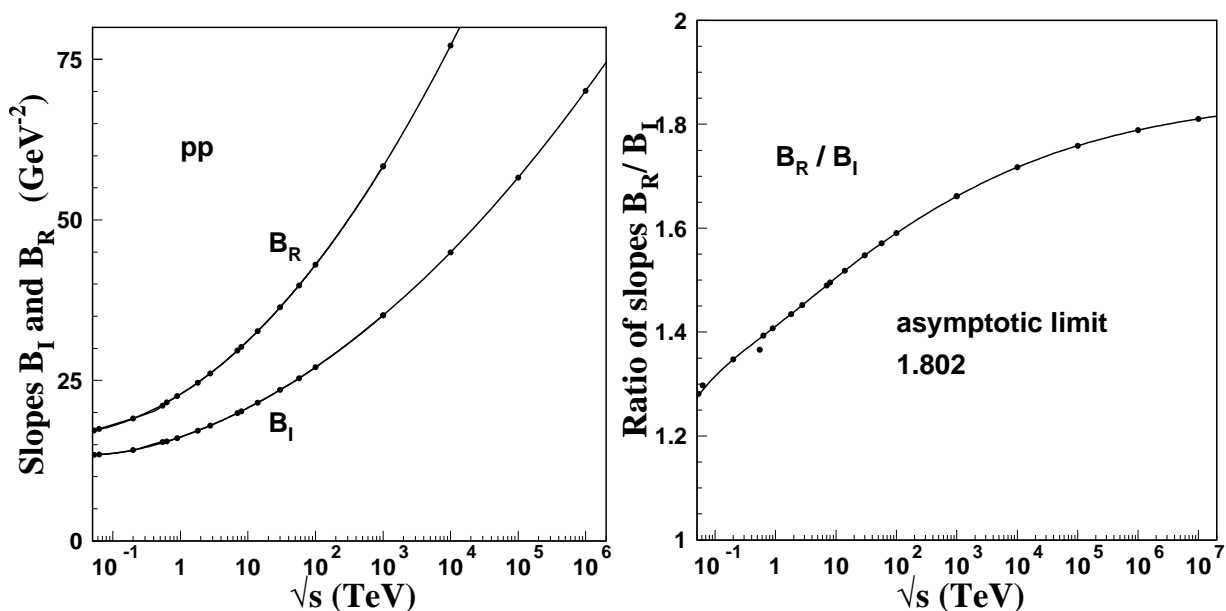


FIG. 1. The slopes of the imaginary and real parts of the amplitude increase with the energy as  $\log^2 \sqrt{s}$ , always with  $B_R > B_I$ . The asymptotic value of the ratio is 1.802.

In terms of the eikonal function  $\chi(s, \vec{b})$  this is written

$$-i \widehat{T}_{pp}(s, \vec{b}) = 1 - e^{i\chi_{pp}(s, \vec{b})} \equiv \Gamma_{pp}(s, \vec{b}) . \quad (11)$$

The term  $e^{i\chi_{pp}(s, \vec{b})}$  represents the S-matrix function in  $b$ -space. The optical theorem for pp scattering appears as

$$\sigma_{pp}^{\text{tot}}(s) = 2 (\hbar c)^2 \Re \int d^2\vec{b} \Gamma_{pp}(s, \vec{b}) . \quad (12)$$

Analogously, for elastic scattering in the p-A system, we define a quantity  $\Gamma_{pA}(s, \vec{b})$  that satisfies the optical theorem for the pA total cross section

$$\sigma_{pA}^{\text{tot}}(s) = 2 (\hbar c)^2 \Re \int d^2\vec{b} \Gamma_{pA}(s, \vec{b}) . \quad (13)$$

Glauber theory introduces a structure to express  $\Gamma_{pA}(s, \vec{b})$  in terms of pp scattering amplitudes and reaction matrix elements.

To describe the phenomena in the Extensive Air Showers (EAS) in Cosmic Ray (CR) observations we need to evaluate the quantity

$$\sigma_{p\text{-air}}^{\text{prod}} = \sigma_{p\text{-air}}^{\text{tot}} - (\sigma_{p\text{-air}}^{\text{el}} + \sigma_{p\text{-air}}^{\text{q-el}}) \quad (14)$$

that is determined experimentally. The quantities named p-air are averages over a mixture of nitrogen and oxygen nuclei.

For elastic and quasi-elastic processes characterized by momentum transfer  $|t|$ , a transition matrix element between states  $i$  and  $f$ , defined with nucleon coordinates  $(\vec{r}_1, \dots, \vec{r}_A)$  is written

$$\begin{aligned} -i T_{pA}^{fi}(s, q^2) &= \frac{1}{2\pi} \int d^2\vec{b} e^{ic\vec{q}\cdot\vec{b}} \int \psi_f^*(\vec{r}_1, \dots, \vec{r}_A) \\ &\times \Gamma_{pA}(s, \vec{b}, \vec{s}_1, \dots, \vec{s}_A) \psi_i(\vec{r}_1, \dots, \vec{r}_A) \prod_{j=1}^A d^3\vec{r}_j , \end{aligned} \quad (15)$$

with  $\vec{b}$  the p-A impact parameter,  $\vec{r}_i$  the position of the nucleon inside the nucleus,  $\vec{s}_i$  the projection of  $\vec{r}_i$  in the perpendicular collision plane.

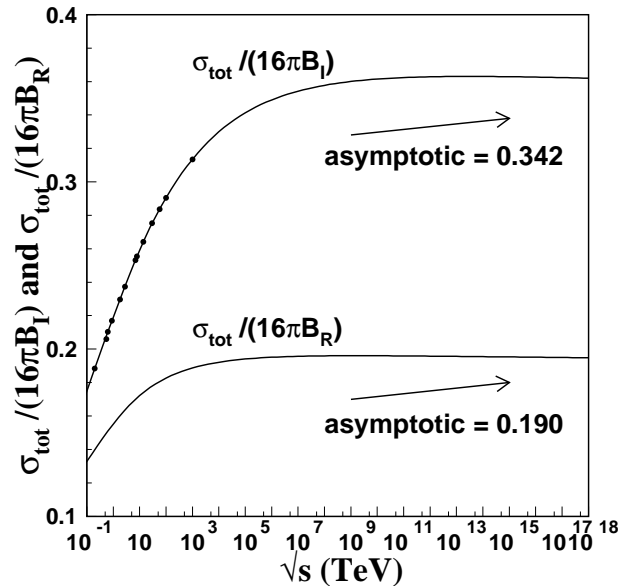


FIG. 2. Energy dependence of the dimensionless ratios between total pp cross section and the slopes  $B_L$  and  $B_R$ , as defined by Eqs. (7, 9). The expressions have finite asymptotic limits, as shown in equations and in the plots.

Glauber method introduces for p-A scattering the expression based on product of S-matrix factors of  $A$  independent elementary scattering processes

$$\Gamma_{\text{pA}}(s, \vec{b}, \vec{s}_1, \dots, \vec{s}_A) = 1 - \prod_{j=1}^A \left[ 1 - \Gamma_{\text{pp}}(s, |\vec{b} - \vec{s}_j|) \right]. \quad (16)$$

This is an assumption of a factorization property for the p-A system.

Then the expression for the transition matrix element becomes

$$T_{\text{pA}}^{fi}(s, q^2) = \frac{1}{2\pi} \int d^2\vec{b} e^{ic\vec{q}\cdot\vec{b}} \int \psi_f^*(\vec{r}_1, \dots, \vec{r}_A) \times \quad (17)$$

$$\left[ 1 - \prod_{j=1}^A \left[ 1 - \Gamma_{\text{pp}}(s, |\vec{b} - \vec{s}_j|) \right] \right] \psi_i(\vec{r}_1, \dots, \vec{r}_A) \prod_{j=1}^A d^3\vec{r}_j. \quad (18)$$

The sum of elastic and quasi-elastic processes is given by

$$\begin{aligned} \sigma_{\text{pA}}^{\text{el}} + \sigma_{\text{pA}}^{\text{q-el}} &= (\hbar c)^2 \int d^2\vec{q} \sum_f |T_{\text{pA}}^{fi}(s, q^2)|^2 \quad (19) \\ &= (\hbar c)^2 \int d^2\vec{q} \sum_f \left| \frac{1}{2\pi} \int d^2\vec{b} e^{ic\vec{q}\cdot\vec{b}} \int \psi_f^*(\vec{r}_1, \dots, \vec{r}_A) \times \right. \\ &\quad \left. \left[ 1 - \prod_{j=1}^A \left[ 1 - \Gamma_{\text{pp}}(s, |\vec{b} - \vec{s}_j|) \right] \right] \psi_i(\vec{r}_1, \dots, \vec{r}_A) \prod_{k=1}^A d^3\vec{r}_k \right|^2 \\ &= (\hbar c)^2 \int d^2\vec{b} \times \\ &\quad \int \left| 1 - \prod_{j=1}^A \left[ 1 - \Gamma_{\text{pp}}(s, |\vec{b} - \vec{s}_j|) \right] \right|^2 \prod_{k=1}^A \rho_k(\vec{r}_k) d^3\vec{r}_k \\ &\equiv (\hbar c)^2 \int d^2\vec{b} \frac{d\sigma_{\text{pA}}^{\text{el+q-el}}}{d^2\vec{b}}(s, b). \end{aligned}$$

In Eq. (19) we have made use of the orthogonality condition

$$\int \psi_f^*(\vec{r}_1, \dots, \vec{r}_A) \psi_i(\vec{r}_1, \dots, \vec{r}_A) \prod_{j=1}^A d^3\vec{r}_j = 0, \quad (20)$$

the completeness relation

$$\sum_f \psi_f^*(\vec{r}_1, \dots, \vec{r}_A) \psi_f(\vec{r}_1', \dots, \vec{r}_A') = \prod_{j=1}^A \delta(\vec{r}_j - \vec{r}_j') \quad (21)$$

and the definition of the nucleon densities  $\rho_k(\vec{r}_k)$ .

Assuming that the  $i$  and  $f$  states are similar bound nuclei with nucleon densities  $\rho_j(\vec{r}_j)$ , and that there is no correlation between the nucleons in the collision process, we write

$$\psi_i^*(\vec{r}_1, \dots, \vec{r}_A) \psi_i(\vec{r}_1, \dots, \vec{r}_A) = \prod_{j=1}^A \rho_j(\vec{r}_j), \quad (22)$$

where  $\rho_j(\vec{r}_j)$  is the density of the nucleon  $j$  in the nucleus.

For atoms with atomic numbers  $A$  less than or equal 18 typically present in the atmosphere the nuclear densities can be described by harmonic potentials with s and p orbitals  $\rho_s(\vec{b})$  and  $\rho_p(\vec{b})$  that are introduced explicitly [11] as

$$\begin{aligned} \rho_s(\vec{r}) &= \frac{1}{\pi^{3/2} b_0^3} e^{-r^2/b_0^2} \quad (23) \\ \rho_p(\vec{r}) &= \frac{2r^2}{3\pi^{3/2} b_0^5} e^{-r^2/b_0^2}, \end{aligned}$$

normalized to unity

$$\int d^3\vec{r} \rho_{s,p}(\vec{r}) = 1 . \quad (24)$$

In this work, for nitrogen and oxygen nuclei the parameters are  $b_0 = 1.7069$  fm and  $b_0 = 1.8133$  fm respectively.

Taking the product of Eq.(19) over the nuclear densities, with 4 nucleons in s shell and A-4 in p shell, we have

$$\begin{aligned} \sigma_{pA}^{\text{el}} + \sigma_{pA}^{\text{q-el}} &= (\hbar c)^2 \int d^2\vec{b} \times \\ &\left\{ 1 - 2\Re \left[ \left[ \int d^3\vec{r} (1 - \Gamma_{pp}(\vec{b} - \vec{s})) \rho_s(r) \right]^4 \times \right. \right. \\ &\left. \left[ \int d^3\vec{r} (1 - \Gamma_{pp}(\vec{b} - \vec{s})) \rho_p(r) \right]^{A-4} \right] \\ &+ \left[ \int d^3\vec{r} (1 - 2\Re \Gamma_{pp}(\vec{b} - \vec{s}) + |\Gamma_{pp}(\vec{b} - \vec{s})|^2) \rho_s(\vec{r}) \right]^4 \times \\ &\left. \left[ \int d^3\vec{r} (1 - 2\Re \Gamma_{pp}(\vec{b} - \vec{s}) + |\Gamma_{pp}(\vec{b} - \vec{s})|^2) \rho_p(\vec{r}) \right]^{A-4} \right\} . \end{aligned} \quad (25)$$

The quantity that enters Eq. (13) for the evaluation of the total pA cross section is

$$\begin{aligned} \Gamma_{pA}(s, \vec{b}) \\ = 1 - \prod_{j=1}^A \int d^3\vec{r}_j \rho_j(\vec{r}_j) \left[ 1 - \Gamma_{pp}(s, |\vec{b} - \vec{s}_j|) \right] . \end{aligned} \quad (26)$$

and the pA total cross section is given by

$$\begin{aligned} \sigma_{pA}^{\text{tot}}(s) &= 2 (\hbar c)^2 \Re \int d^2\vec{b} \times \\ &\left( 1 - \prod_{j=1}^A \int d^3\vec{r}_j \rho_j(\vec{r}_j) \left[ 1 - \Gamma_{pp}(s, |\vec{b} - \vec{s}_j|) \right] \right) \\ &\equiv (\hbar c)^2 \int d^2\vec{b} \frac{d\tilde{\sigma}_{pA}^{\text{tot}}}{d^2\vec{b}}(s, b) . \end{aligned} \quad (27)$$

For p-A elastic scattering we have

$$\begin{aligned} \sigma_{pA}^{\text{el}}(s) &= (\hbar c)^2 \int |T_{pA}^{ii}(s, q^2)|^2 d^2\vec{q} \\ &= (\hbar c)^2 \int \left| \frac{1}{2\pi} \int d^2\vec{b} e^{ic\vec{q}\cdot\vec{b}} \int \psi_i^*(\vec{r}_1, \dots, \vec{r}_A) \times \right. \\ &\left. \left[ 1 - \prod_{j=1}^A \left[ 1 - \Gamma_{pp}(s, |\vec{b} - \vec{s}_j|) \right] \right] \psi_i(\vec{r}_1, \dots, \vec{r}_A) \prod_{j=1}^A d^3\vec{r}_j \right|^2 d^2\vec{q} \\ &= (\hbar c)^2 \int d^2\vec{b} \left| 1 - \prod_{j=1}^A \int d^3\vec{r}_j \rho_j(\vec{r}_j) \left[ 1 - \Gamma_{pp}(s, |\vec{b} - \vec{s}_j|) \right] \right|^2 \\ &= (\hbar c)^2 \int d^2\vec{b} \left| \Gamma_{pA}(s, \vec{b}) \right|^2 \equiv (\hbar c)^2 \int d^2\vec{b} \frac{d\tilde{\sigma}_{pA}^{\text{el}}}{d^2\vec{b}}(s, b) . \end{aligned} \quad (28)$$

We thus follow Glauber formalism [8] in general lines, with independent slopes  $B_R$  and  $B_I$ . We consider also the effect of the contributions of intermediate diffractive states according to Good-Walker [9], with a parameter  $\lambda$ . For

practical implementation [10] we re-write Eq.(26) as

$$\Gamma_{pA}(s, \vec{b}, \vec{s}_1, \dots, \vec{s}_A) = 1 - \frac{1}{2} \prod_{j=1}^A \left[ 1 - (1 + \lambda) \Gamma_{pp}(\vec{b} - \vec{s}_j) \right] - \frac{1}{2} \prod_{j=1}^A \left[ 1 - (1 - \lambda) \Gamma_{pp}(\vec{b} - \vec{s}_j) \right], \quad (29)$$

and consequently modify Eqs.(13) and (25).

Stressing that we provide reliable information on cross sections and amplitude slopes for the pp scattering input, and a proper, although simple, treatment of Glauber framework, we believe that our calculations of  $\sigma_{p\text{-air}}^{\text{prod}}$  are worth as a study of the EAS data. Actually, we show in the next section that there is very good coherence between our calculations and the data.

The dimensionless quantities that give the  $b$ -dependence of the total, elastic+quasi-elastic and pure elastic cross sections for the p-air system (taking averages over nitrogen and oxygen components)

$$\frac{d\tilde{\sigma}_{p\text{-air}}^{\text{tot}}}{d^2\vec{b}}(s, b), \quad \frac{d\tilde{\sigma}_{p\text{-air}}^{\text{el+q-el}}}{d^2\vec{b}}(s, b), \quad \frac{d\tilde{\sigma}_{p\text{-air}}^{\text{el}}}{d^2\vec{b}}(s, b) \quad (30)$$

are represented in Fig. 3 for the energies  $\sqrt{s} = 57$  and  $\sqrt{s} = 1000$  TeV. As in the pp system, the total and inelastic cross sections for small  $b$  approach the limits 2 and 1 as the energy increases. There is little difference between the elastic+quasi-elastic and the pure elastic quantities.

The integrated quantities  $\sigma_{p\text{-air}}^{\text{tot}}(s)$ ,  $\sigma_{p\text{-air}}^{\text{el}} + \sigma_{p\text{-air}}^{\text{q-el}}(s)$  and  $\sigma_{p\text{-air}}^{\text{el}}(s)$  are shown in the second part of the same figure. The ratio  $\sigma_{p\text{-air}}^{\text{el}}/\sigma_{p\text{-air}}^{\text{tot}}$  is 0.33 at 57 TeV and 0.35 at 1000 TeV. The difference between elastic+quasi-elastic and purely elastic contributions is remarkably small, of about 18 % at 50 GeV and falling steadily to zero as the energy increases. The inelastic p-air cross section is about 2/3 of the total, as in the pp system.

#### IV. COMPARISON WITH DATA

Fig. 4 shows our calculation of  $\sigma_{p\text{-air}}^{\text{prod}}$  with a solid line, together with the data points from experiments with Extensive Air Showers [12–19].

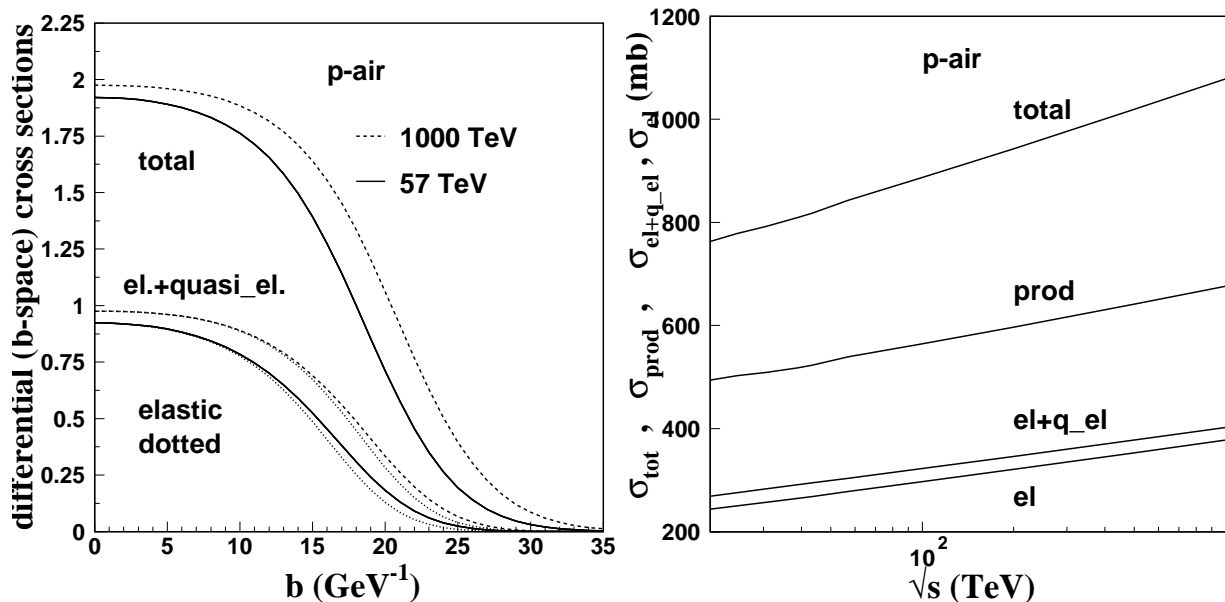


FIG. 3. The quantities  $d\sigma_{p\text{-air}}^{\text{tot}}/d^2\vec{b}$  and  $d\sigma_{p\text{-air}}^{\text{el+q-el}}/d^2\vec{b}$  are plotted as functions of the p-air impact parameter  $b$  for the energies 57 and 1000 TeV. As the energy increases, the saturation limits 2 and 1 are approached by the total and inelastic parts for small  $b$ . The integrated quantities are shown in the second part of the figure. The small difference between elastic+quasi-elastic and purely elastic terms is remarkable.

The procedure is straightforward and unique, without free parameters, made with inputs given by our model for the pp interaction that describes the elastic differential cross sections at all energies from 20 GeV to 8 TeV in the whole  $t$ -range, with high precision. For the application in Glauber calculation of the p-air processes in the EAS experiments, the model enters only in its forward scattering limit, and is represented by Eqs. (2-5). The log-squared increases of  $\sigma$ ,  $B_I$ ,  $B_R$  are consequence of the Yukawa-like behaviour of the amplitudes, and do not violate unitarity or dispersion relations [3]. Thus we consider that this is a reliable input.

The calculation of  $\sigma_{p\text{-air}}^{\text{prod}}$  is made with Eq. (14), as explained in the previous section. The figure shows that in general there is good agreement, without systematic deviation that could require additional term in Eq. (14) that would be beyond the basic Glauber form. At high energies above 10 TeV ( $\sqrt{s}$  in the proton-proton system) the agreement is particularly satisfactory, considering the quality of the present experimental information. In the low energy region we observe that data from the ARGO-YBJ experiment [17] is below the theoretical curve, while the data from the Kaskade experiment [18] do not shown the same systematic deviation.

The theoretical curve for the production cross section can be put in the simple and convenient form

$$\sigma_{p\text{-air}}^{\text{prod}} = 383.474 + 33.158 \log \sqrt{s} + 1.3363 \log^2 \sqrt{s} , \quad (31)$$

with  $\sqrt{s}$  in TeV.

We observe that the data and our calculations of  $\sigma_{p\text{-air}}^{\text{prod}}$  increase with similar  $\log^2 \sqrt{s}$  energy dependence as the pp cross sections, but more slowly. To compare the two rates and give more evidence of regularity in the data, we show in Fig. 5 the relation  $\sigma_{p\text{-air}}^{\text{prod}}/\sigma(\text{pp})$  for a set of selected data (chosen by regularity reasons) together with our calculations. The ratio decreases regularly, approaching a finite and distant asymptotic limit, as pointed out by the relation of forms in Eqs. (31) and (2). The importance of the existence of a finite asymptotic limit for this ratio and its numerical value at ultra-high energies are discussed in a geometric approach in Sec.5.

We hope that this observation of regularity and interesting energy dependence of this ratio will be confirmed by more measurements and will help the understanding of the hadronic interactions in cosmic ray experiments.

Other models of the pp interaction [20] have different features, such as the energy dependence of the slopes and their correlation with the total cross section, and the behaviour of the inelastic pp cross section (in our model we have at high energies  $\sigma^{\text{inel}}/\sigma^{\text{tot}} = 2/3$  while the black disk value is 1/2). The use of these models as pp inputs may lead to systematic deviations with respect to data, and may lead to suggestions of additional contributions to the quantity  $\sigma_{p\text{-air}}^{\text{prod}}$  written in Eq. (14). Thus, as a historical example, the data of Akeno [15] and Fly's Eye [14] in the 30 TeV region was studied critically [20–22] in efforts to identify contributions that could influence the determination of the pp total cross section. The measured values of  $\sigma_{p\text{-air}}^{\text{prod}}$  were both apparently too high, leading (using models for the sigma/slope correlation) to values of pp cross section then considered too large. The Akeno value at  $\sqrt{s} = 24.54$  TeV is  $550 \pm 72$  mb , and the Fly's Eye measurement at  $\sqrt{s} = 30.0$  TeV is  $530 \pm 66$  mb . As seen in Fig. 4 our calculation

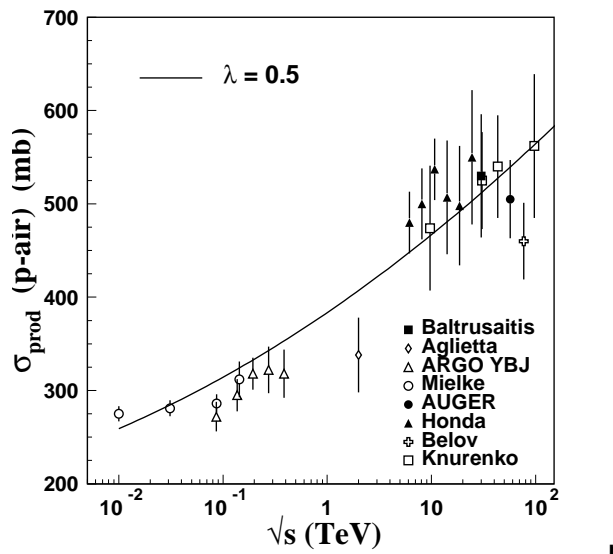


FIG. 4. Our calculation of the p-air production cross section is represented by the solid line, that is well represented by Eq. (31). Details are given in the text. The data are from several experiments [12–19]. Both data and calculations increase with the energy with a  $\log^2 \sqrt{s}$  form.

TABLE I. Influences of the quantities  $\lambda$  and  $B_R$  in Glauber calculations of  $\sigma_{p\text{-air}}$  at  $\sqrt{s} = 57$  TeV. The input parameters are  $\sigma = 140.66$  mb,  $B_I = 25.33$  GeV $^{-2}$ ,  $B_R = 39.80$  GeV $^{-2}$  and  $\rho = 0.132$ . Some data points are included to provide a scale for the importance of the effects in comparison to experimental errors. The effects increase with the energy, and may become important as experimental errors decrease.

$\lambda$	$B_I$	$B_R$	$\sigma_{p\text{-air}}^{\text{prod}}$
0.5	25.329	39.796	539.225
0.5	25.329	25.329	536.617
0.0	25.329	39.796	537.547
0.0	25.329	25.329	537.333

also considers these values of production as too high. A critical analysis of the interpretation of the experiments [22] showed that the reported values for  $\sigma_{p\text{-air}}^{\text{prod}}$  should be reduced. Actually, a later measurement [16] of the Yakutsk Array experiment obtained a comparatively lower value  $525 \pm 52$  mb at 30.65 GeV that is closer to our prediction of 509 mb. Contributions due to processes of excitation of nucleon isobars [20], that were estimated as being at about 3 %, are not considered in other calculations [21, 22]. These measurements and analyses in the 30 TeV region are an example of difficulties in the interpretation of EAS data.

Fig. 6 shows the influences of the difference of values  $B_R \neq B_I$  and of the quantity  $\lambda$  that represents the presence of diffractive intermediate states, which is tested with values 0 and 0.5 [10, 12]. As we see, the effects do not appear as large in the plots, increase with the energy, and may become more important as experimental errors and oscillations decrease. The value  $\lambda = 0.5$  is assumed to represent the measurement of  $\sigma^{\text{SD}}/\sigma_{\text{inel}}$  from ISR. This value could be updated with LHC measurements.

Table I shows comparative numbers for several cases at the energy 57 TeV, where we see that the effects on values of the p-air cross section are under 1 percent. In the  $B_R$  case the weak influence is due to the small  $\rho$  value.

The confrontation of our calculation with data at high energies does not indicate the need of contributions beyond the standard Glauber calculation. However, the EAS data are not regular and have large error bars, due to uncertainties in the extraction of values for  $\sigma_{p\text{-air}}^{\text{prod}}$ . Improvement in the quality of future data may indicate influence of processes occurring in intermediate states of the p-air collision, as nucleon excitations, correlations, shadowing. A particular example is given by the recent AUGER measurement at 57 TeV, that seems a bit too low with respect to the general trend of the data, and has been published with large error bars.

In the low energy region, the data of the ARGO YBJ collaboration [17] there may be a regular deviation of our calculations. It may be that same effects that are not observable at 100 TeV may become important in this range. Anyhow, the discrepancies are not large, amounting to a maximum of 10% : at  $\sqrt{s} = 0.0865$  TeV the ARGO YBJ

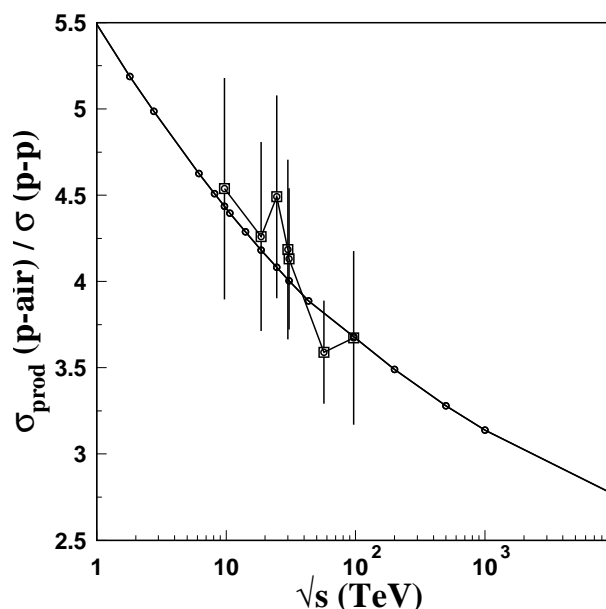


FIG. 5. Ratio of p-air and pp cross sections. We show our calculation in solid line (with dots) together with selected data. We observe regular behaviour in the energy variation of the data, that slowly approaches a finite asymptotic limit.

experiment gives  $\sigma_{p\text{-air}}^{\text{prod}} = 272 \pm 15.8$  mb , while the theory gives 307.21 mb. On the contrary, at  $\sqrt{s} = 0.031$  TeV the Kaskade experiment [18] and the theoretical value coincide very well (at  $281 \pm 8.5$  and 286 mb respectively).

In general, there seems to be more room for improvement in the measurements than in our theoretical calculation, and we believe that our pp input together with the basic Glauber calculation have successfully passed the test in the comparison with EAS data.

## V. GEOMETRIC VIEW AND ASYMPTOTIC APPROACH

An important feature of our pp scattering amplitude is its large- $b$  behaviour. Writing the  $b$  integrated cross section as

$$\sigma(s) = \int d^2\vec{b} \frac{d\sigma}{d^2\vec{b}}, \quad (32)$$

we observe that the integrand,  $d\sigma/d^2\vec{b}$ , as function of  $b$  present a long range tail, rather than a sharp cut-off, that is the characteristic of a black disk model[3]. This behaviour survives at asymptotic energies, presenting a scaling property as shown in Fig. 7. In the left side of this figure we show  $d\sigma_{pp}^{\text{tot}}/d^2\vec{b}$  as function of  $b$  for three different energies. When these curves are plotted as function of scaled variable  $x = b/\sqrt{\sigma(\sqrt{s})/2\pi}$ , three curves almost degenerate to a unique curve as shown in the right side of this figure. Such a property is known as "geometrical scaling law", advocated by J. Dias de Deus, a long time ago. [24].

To make clear how this geometrical scaling nature affects in pp and pA cross sections, let us first summarize the simplified Glauber picture below. When we write the elastic pp scattering amplitude as the form Eq.(11),

$$-i \hat{T}_{pN}(s, \vec{b}) = 1 - e^{i\chi(s, \vec{b})}, \quad (33)$$

the last term is essentially the  $S$ -matrix in  $b$  space. For high energies,  $b$  represents essentially the angular momentum, so that  $\chi$  is (a twice of) the phase shift. In the presence of inelastic channels,  $\chi$  becomes complex,  $\chi = \chi_R + i\chi_I$ , and

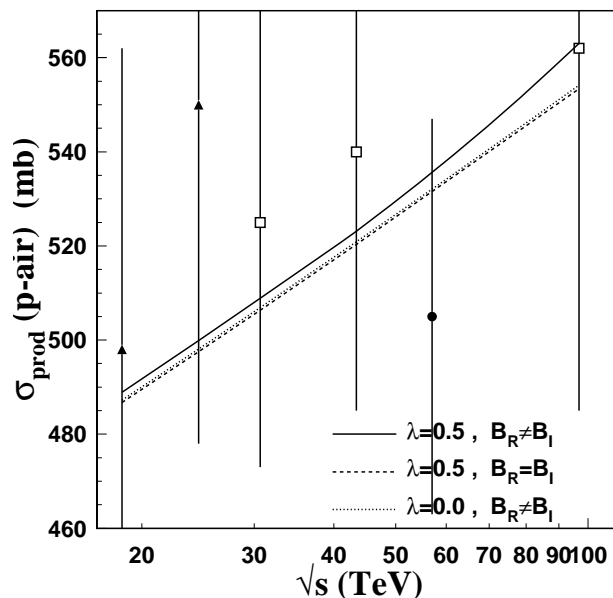


FIG. 6. Effects of the values of the parameter  $\lambda$  of the Good-Walker formalism with intermediate states and of the difference of values between imaginary and real slopes in Glauber calculation. The solid line represents the calculation with  $\lambda = 0.5$ . The dashed and dotted lines, very close to each other, represent modified calculations putting  $\lambda = 0$ , in dotted line, and putting  $B_R = B_I$ , in dashed line. Some data points are shown together to help the information on the magnitude of the effects.

we can define the impact parameter representation of partial cross sections in terms of these functions as

$$\frac{d^2\sigma_{pp}^{\text{el}}}{d^2\vec{b}} = 1 - 2 \cos \chi_R e^{-\chi_I} + e^{-2\chi_I}, \quad (34)$$

$$\frac{d^2\sigma_{pp}^{\text{inel}}}{d^2\vec{b}} = 1 - e^{-2\chi_I}, \quad (35)$$

$$\frac{d^2\sigma_{pp}^{\text{tot}}}{d^2\vec{b}} = 2(1 - \cos \chi_R e^{-\chi_I}). \quad (36)$$

At high energies, for the calculation of total and integrated cross sections, we can safely take  $\chi_R \rightarrow 0$ , so that

$$\sigma_{pp}^{\text{el}}(s) \rightarrow \int d^2\vec{b} (1 - e^{-\chi_I})^2, \quad (37)$$

$$\sigma_{pp}^{\text{inel}}(s) \rightarrow \int d^2\vec{b} (1 - e^{-2\chi_I}), \quad (38)$$

$$\sigma_{pp}^{\text{tot}}(s) \rightarrow 2 \int d^2\vec{b} (1 - e^{-\chi_I}). \quad (39)$$

The Glauber approximation consists in writing the pA S-matrix as a simple product of independent scattering centers inside the nucleus,

$$e^{i\chi_{pA}} \simeq \left\langle \prod_{j=1}^A e^{i\chi_{pN_j}} \right\rangle \quad (40)$$

where  $\langle \rangle$  denotes the average over all nucleon states inside the nucleus and the product  $\prod_i$  is taken over the nucleons  $N_j$ . Thus, the pA scattering amplitude is

$$\begin{aligned} -i\widehat{T}_{pA}(\vec{b}) &= 1 - e^{i\chi_{pA}} \\ &\simeq 1 - \left\langle \prod_{j=1}^A e^{i\chi_{pN_j}} \right\rangle \\ &= 1 - \left\langle \prod_{j=1}^A (1 + i\widehat{T}_{pN}(\vec{b})) \right\rangle, \end{aligned} \quad (41)$$

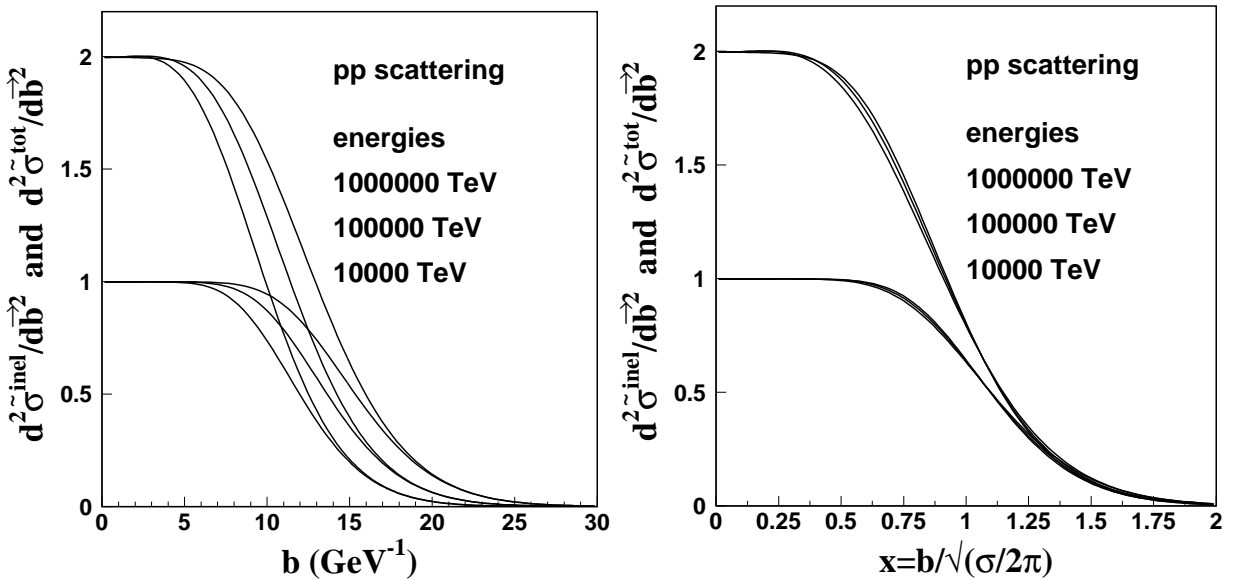


FIG. 7. Dimensionless differential  $b$ -space cross sections for total and inelastic pp interactions. The plotted energies are  $10^4$ ,  $10^5$  and  $10^6$  TeV. In the second part of the figure, the cross sections are plotted against the scaled variable  $x$ , showing universal behaviour, as explained in the text.

that leads to equations of last section. Glauber approach gives essentially

$$\begin{aligned} & \frac{1}{2} \frac{d^2 \sigma_{pA}^{\text{tot}}}{d^2 \vec{b}}(s, \vec{b}) \\ &= \left\langle 1 - \prod_{i=1}^A \left( 1 - \frac{1}{2} \frac{d^2 \sigma_{pp}^{\text{tot}}}{d^2 \vec{b}_i}(s, \vec{b} - \vec{b}_i) \right) \right\rangle, \end{aligned} \quad (42)$$

and

$$\begin{aligned} & \frac{d^2 \sigma_{pA}^{\text{el}}}{d^2 \vec{b}}(s, \vec{b}) \\ &= \left\langle \left[ 1 - \prod_{i=1}^A \left( 1 - \frac{d^2 \sigma_{pp}^{\text{tot}}}{d^2 \vec{b}_i}(s, \vec{b} - \vec{b}_i) \right) \right]^2 \right\rangle. \end{aligned} \quad (43)$$

At extremely high energies,  $\sigma_{pp}^{\text{tot}}$  may become much larger than the geometrical cross section of the target nucleus,  $\sigma_A^{\text{geo}} \equiv \pi R_A^2$ , where  $R_A$  is the nuclear radius. In such a situation we may neglect the variation in position of each nucleon ( $\vec{b}_i \sim 0$ ), and we can approximate

$$\frac{1}{2} \frac{d^2 \sigma_{pA}^{\text{tot}}}{d^2 \vec{b}}(s, \vec{b}) \simeq 1 - \left( 1 - \frac{1}{2} \frac{d^2 \sigma_{pp}^{\text{tot}}}{d^2 \vec{b}}(s, \vec{b}) \right)^A, \quad (44)$$

and

$$\frac{d^2 \sigma_{pA}^{\text{el}}}{d^2 \vec{b}}(s, \vec{b}) \simeq \left[ 1 - \left( 1 - \frac{d^2 \sigma_{pp}^{\text{tot}}}{d^2 \vec{b}}(s, \vec{b}) \right)^A \right]^2. \quad (45)$$

Such situation can occur in our case only for  $\sqrt{s} \gg 10^{12}$  TeV, much larger than the highest energy observed in cosmic ray experiments.

Now, as shown in Fig. (7), our amplitudes lead to an approximate geometric scaling law for very large energies,

$$\frac{1}{2} \frac{d\sigma_{pp}^{\text{tot}}}{d^2 \vec{b}}(s, \vec{b}) \rightarrow \zeta(x), \quad (46)$$

where  $\zeta$  is an universal function independent of  $\sqrt{s}$  and

$$x \equiv \frac{b}{b_{eff}(\sqrt{s})}, \quad (47)$$

with  $b_{eff}(\sqrt{s}) \sim \sigma(\sqrt{s})$ . The total pp cross section then becomes

$$\sigma_{pp}^{\text{tot}}(s) \rightarrow 4\pi b_{eff}^2(\sqrt{s}) \int_0^\infty x \zeta(x) dx. \quad (48)$$

If we introduce another function

$$\xi(x) = 1 - [1 - \zeta(x)]^2, \quad (49)$$

to write the inelastic cross section as

$$\sigma_{pp}^{\text{inel}}(s) \rightarrow 2\pi b_{eff}^2(\sqrt{s}) \int_0^\infty x \xi(x) dx, \quad (50)$$

where we have used Eqs. (38, 39). From Eqs.(48, 50), we obtain

$$\frac{\sigma_{pp}^{\text{inel}}(s)}{\sigma_{pp}^{\text{tot}}(s)} \rightarrow \frac{\int_0^\infty x \xi(x) dx}{2 \int_0^\infty x \zeta(x) dx} = \text{const.} \quad (51)$$

As shown in Fig.(7),  $\zeta$  and  $\xi$  are functions having a common property,

$$\zeta(x), \xi(x) \rightarrow \begin{cases} 1, & x \rightarrow 0 \\ 0, & x \rightarrow \infty \end{cases}, \quad (52)$$

When we have the case of a sharp cut-off of  $\zeta$  as in a black disk

$$\zeta(x) = \theta(1-x), \quad (53)$$

then  $\xi(x)$  becomes identical with  $\zeta(x)$ , and we have the ratio

$$\lim_{s \rightarrow \infty} \frac{\sigma_{pp}^{\text{inel}}(s)}{\sigma_{pp}^{\text{tot}}(s)} = \frac{1}{2}, \quad (54)$$

that is a well known result for a black disk.

Generally,  $\zeta(x)$  is not a sharp-cut theta function as in Eq. (53) but stays unity up to a certain value of  $x$  (that is  $x = 1, b = b_{eff}(\sqrt{s})$ ), then monotonically decreases to zero with a tail form. Let us write then

$$\zeta(x) = \begin{cases} 1, & x \leq 1 \\ \Phi(x), & x > 1 \end{cases}, \quad (55)$$

where  $\Phi(x)$  is a positive and monotonically decreasing function with  $\Phi(1) = 1$ .

Let us now turn to the pA case. From Eqs. (44, 45), we have

$$\frac{1}{2}\sigma_{pA}^{\text{tot}}(s) = 2\pi b_{eff}^2(\sqrt{s}) \int_0^\infty x dx \left[1 - (1 - \zeta(x))^A\right], \quad (56)$$

and

$$\sigma_{pA}^{\text{el}}(s) = 2\pi b_{eff}^2(\sqrt{s}) \int_0^\infty x dx \left[1 - (1 - \zeta(x))^A\right]^2, \quad (57)$$

so that, taking the difference  $\sigma_{pA}^{\text{tot}} - \sigma_{pA}^{\text{el}}$ ,

$$\begin{aligned} \sigma_{pA}^{\text{inel}}(s) &= 2\pi b_{eff}^2(\sqrt{s}) \int_0^\infty x dx \left[1 - (1 - \zeta(x))^{2A}\right] \\ &= 2\pi b_{eff}^2(\sqrt{s}) \left(\frac{1}{2} + \int_1^\infty x dx \left[1 - (1 - \Phi(x))^{2A}\right]\right). \end{aligned} \quad (58)$$

Since  $0 \leq 1 - \Phi \leq 1$  for all  $x$ , we have  $(1 - \Phi)^{2A} \leq 1 - \Phi$ , for  $A \geq 1$ . Thus we have the inequality

$$\int_1^\infty x dx \left(1 - (1 - \Phi(x))^{2A}\right) \geq \int_1^\infty x dx \Phi(x). \quad (59)$$

From this consideration, we arrive at the conclusion that

$$\begin{aligned} \frac{\sigma_{pA}^{\text{inel}}}{\sigma_{pp}^{\text{tot}}}(s) &= \int_0^\infty x dx \left[1 - (1 - \zeta(x))^{2A}\right] / \int_0^\infty 2x \zeta(x) dx \\ &\geq 1/2, \end{aligned} \quad (60)$$

for  $\sqrt{s} \rightarrow \infty$ . Note that in the black disk case  $\Phi(x) \equiv 0$ , or equivalently  $\zeta(x) = \theta(1-x)$ , we obtain the well-defined limit

$$\sigma_{pA}^{\text{inel}}(s)/\sigma_{pp}^{\text{tot}}(s) \rightarrow \frac{1}{2}.$$

As a corollary to Eq.(60), for two different target nuclei  $A$  and  $A'$ , with for  $A < A'$  and  $\zeta(x) \neq \theta(x)$  we have the inequality

$$\frac{\sigma_{pA}^{\text{inel}}}{\sigma_{pp}^{\text{tot}}}(s) < \frac{\sigma_{pA'}^{\text{inel}}}{\sigma_{pp}^{\text{tot}}}(s). \quad (61)$$

Naturally Eq.(60) is valid also for  $A = 1$  and in this case

$$\frac{\sigma_{pp}^{\text{inel}}}{\sigma_{pp}^{\text{tot}}}(s) = \frac{1 + 2 \int_1^\infty x dx \left[1 - (1 - \Phi(x))^2\right]}{2 \left(1 + 2 \int_1^\infty x dx \Phi(x)\right)} > \frac{1}{2}, \quad (62)$$

if  $\Phi \neq 0$ . We thus see that the non-black disk nature is intimately related to the tail property  $\Phi(x)$ .

As mentioned before, our phenomenological pp representation does not correspond to the black disk, and the actual pp ratio is  $\sigma_{pp}^{\text{inel}}/\sigma_{pp}^{\text{tot}} \rightarrow 2/3$ . This constraints the tail  $\Phi$ ,

$$\frac{1 + 2 \int_1^\infty x dx \left[1 - (1 - \Phi(x))^2\right]}{2 \left(1 + 2 \int_1^\infty x dx \Phi(x)\right)} = \frac{2}{3}. \quad (63)$$

With this information at hand, we look for an estimate of the value

$$\sigma_{pA}^{\text{inel}}(s)/\sigma_{pp}^{\text{tot}}(s)$$

using a tail form proper for the realistic pp amplitudes.

As a simple choice, considering that the stochastic vacuum model predicts the tail as that of Yukawa behaviour for large  $b$ , we take

$$\zeta(x) = \begin{cases} 1, & x \leq 1 \\ \exp(-\alpha(x-1))/x, & x > 1 \end{cases}, \quad (64)$$

where  $\alpha$  is a parameter to be determined using Eq.(63) In this case, we have

$$\frac{1}{2}\sigma_{pp}^{\text{tot}} = 2\pi b_{eff}^2(\sqrt{s}) \left(\frac{1}{2} + \frac{1}{\alpha}\right), \quad (65)$$

and

$$\xi(x) = \begin{cases} 1, & x \leq 1 \\ 2e^{-\alpha(x-1)}/x - e^{-2\alpha(x-1)}/x^2, & x > 1 \end{cases} \quad (66)$$

to obtain

$$\sigma_{pp}^{\text{inel}} = 2\pi b_{eff}^2(\sqrt{s}) \left(\frac{1}{2} + \frac{2}{\alpha} - \int_0^\infty \frac{e^{-2\alpha x}}{x+1} dx\right) \quad (67)$$

The constraint for  $\alpha$  from Eq.(63) becomes

$$4 \left(\frac{1}{2} + \frac{1}{\alpha}\right) = 3 \left(\frac{1}{2} + \frac{2}{\alpha} - \int_0^\infty \frac{e^{-2\alpha x}}{x+1} dx\right), \quad (68)$$

leading to

$$\alpha \simeq 1.61073. \quad (69)$$

With this, for  $A = 15$ , for example, we obtain

$$\begin{aligned} \sigma_{pA}^{\text{inel}} &= 2\pi b_{eff}^2(\sqrt{s}) \left(1 + \int_1^\infty x dx \left(1 - \frac{e^{-\alpha(x-1)}}{x}\right)^{2A}\right) \\ &\simeq 2\pi b_{eff}^2(\sqrt{s}) \times 2.30764, \end{aligned} \quad (70)$$

giving

$$\left. \frac{\sigma_{pA}^{\text{inel}}}{\sigma_{pp}^{\text{tot}}} \right|_{\text{Yukawa}} \simeq 1.1858. \quad (71)$$

This value depends sensitively on the choice of the tail function  $\Phi$ . The slower the decay of the tail, the bigger the ratio becomes. If we choose  $\Phi$  a pure exponential,

$$\Phi = e^{-\alpha(x-1)}, \quad (72)$$

which is more longer tail than Yukawa type, then using the same procedure to get  $\alpha \simeq 2.1583$  and the corresponding value of the ratio becomes

$$\left. \frac{\sigma_{pA}^{\text{inel}}}{\sigma_{pp}^{\text{tot}}} \right|_{\text{Exponential}} \simeq 1.798. \quad (73)$$

These values of ratio for different tails can be compared with the energy dependence of the ratio shown in Fig. 8 where we plotted the ratio calculated directly by integrating our cross sections numerically for extremely large  $\sqrt{s}$  values up to  $\sqrt{s} = 10^{20}$  TeV. We note that the values are still decreasing, but approaches to a value between those given in Eqs.(71) and (73) .

As we see from this figure, the asymptotic value is only attained only for really large  $\sqrt{s}$ , say  $\sqrt{s} \gg 10^{20}$  TeV. Numerical integration of the cross section at such values of  $\sqrt{s}$  is not trivial due to the huge cancellations, but just to see the tendency, we use the values of  $\sigma_{p\text{-air}}^{\text{inel}}$  at  $10^{12}$ ,  $10^{16}$  and  $10^{20}$  to obtain the extrapolation form

$$\sigma_{p\text{-air}}^{\text{inel}}(s) = 490.883 + 19.7119 \log \sqrt{s} + 1.8178 \log^2 \sqrt{s}. \quad (74)$$

Dividing this function by the  $\log^2$  form of the pp total cross section in Eq. (2), we obtain the dashed line shown in the figure. We see that the representation of the ratio looks very good above  $10^6$  TeV. In this parametrization the predicted asymptotic limit is  $1.8178/1.2273 = 1.4811$  . We would obtain somewhat different limit, had we taken a different set of three energies to construct the form in Eq. (74), but the result would remain in the interval 1.4 - 1.5 . The slow convergence of the ratio towards a finite limit at high energies is an important fact.

The uncertainties given in Eqs.(71) or (73) are due to the form of ansatz,  $\zeta$ . A sharp transition like Eq.(64) at  $x = 1$  is not realistic to our amplitude. However, it is interesting to note that the extrapolated numerical value is in between the values of Eq. (71) and (73), that was determined using as input the 2/3 ratio of inelastic to total pp cross sections and assumption of the Yukawa-like or Exponential tail in the  $b$  dependence of the pp amplitudes.

Eq. (74) gives a proper representation of  $\sigma_{p\text{-air}}^{\text{inel}}(s)$  to be used only for energies higher than  $\sqrt{s} \approx 10^6$  TeV. Nonetheless, when used at the highest CR experimental energy  $\sqrt{s} = 96.85$  it gives a value just 10% larger than the correct one: thus not too bad.

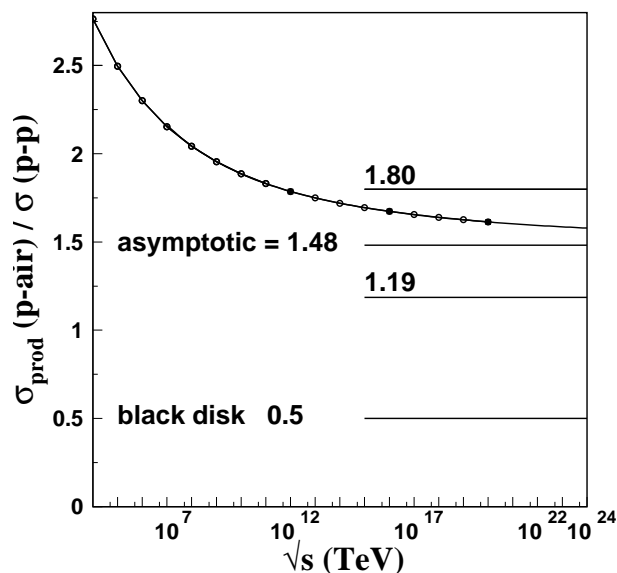


FIG. 8. Ratio of p-air and pp cross sections at ultra-high energies. Calculations are marked with dots and connected with a continuous line. The dashed line is given analytically by the fraction of  $\log^2$  forms for  $\sigma_{p\text{-air}}^{\text{inel}}(s)$  and  $\sigma_{pp}^{\text{tot}}(s)$ , given in the text. It gives good representation of the points for energies above  $10^6$  TeV and tends to the asymptotic limit 1.48, as explained in the text .

On the other hand, the form given for  $\sigma_{\text{p-air}}^{\text{inel}}(s)$  in Eq. (31) is based on the three points  $\sqrt{s} = 96.85, 10^3$  and  $10^4$  TeV, and gives very good representation of the exact values from 10 GeV to  $10^6$  TeV. However, this form is not adequate for the asymptotic limit.

The good coherence of different evaluations of these finite asymptotic ratios is very interesting. They point out to what can be expected for CR experiments at ultra high energies.

## VI. FINAL REMARKS AND COMMENTS

The amplitudes that we have constructed to describe accurately the pp elastic differential cross sections at energies from 20 GeV to 8 TeV are used in Glauber formalism to evaluate the p-air production cross section obtained in EAS/CR experiments. Our prediction for the whole energy interval from 10 GeV to 100 TeV of p-air production cross section is shown in Fig. 4.

The comparison of our results with data shows good agreement, confirming that the extrapolation of the input quantities extrapolated to energies higher by one order of magnitude is consistent. From this we are confident that our representation of pp scattering amplitudes can be used for higher CR data.

The calculations with Glauber approach depend crucially on the input values of  $\sigma_{\text{pp}}^{\text{tot}}(s)$  and  $B_I(s)$ , and thus the results obtained for the high energies of the CR experiments are important tests of the energy dependences that we propose for these quantities, given in Eqs. (2, 3). It is particularly remarkable that the  $\log^2$  dependence that we propose for  $B_I(s)$  predicts higher values for the extrapolated values of this quantity, and the data seem to be consistent with this. Thus at 57 TeV we have  $B_I = 25 \text{ GeV}^{-2}$ , value that is higher than the usual obtained, for example from Donnachie-Landshoff or Regge form. The comparison with CR data helps to test such alternatives.

The extraction of fundamental information on the energy dependence of pp total cross section from CR/EAS measurements depends on this point. Thus our prediction for pp cross section at 57 TeV is of 140.7 mb. In the experimental paper [12], where the measured value for  $\sigma_{\text{p-air}}^{\text{prod}}$  is below our calculation (see Fig. 4), and other theoretical models for  $\sigma(s)$  and  $B_I(s)$  are used, the reported value for  $\sigma$  is  $133 \pm 29$  mb. Hopefully this important question will be investigated in future measurements with cosmic rays.

An important point of our description of differential elastic cross section is that we keep full respect for the real part of the scattering amplitude. The real part is crucial for large  $|t|$  but often neglected in the forward region due to the small value of the  $\rho$  parameter. We stress that the neglect of the proper  $B_R$  value affects the determination of pp total cross section. We take this into account in Glauber calculation of p-air processes. The influence is not large ( $\sim 1\%$  for the total cross section at 57 TeV), but increases with the energy. We have shown in Fig. 6 and in Table I that the effects of the condition  $B_R > B_I$  and of the presence of intermediate diffractive states (parameter  $\lambda$ ) in Good-Walker [9] approach are of similar magnitudes.

From our representation of the scattering amplitudes we can calculate the asymptotic values of quantities that approach finite values at high energies. These values are important for the geometric interpretation of the dynamics, as can be studied in the representation of the impact parameter  $b$ . For example, the behaviour of the ratios  $\sigma_{\text{pp}}^{\text{tot}}/B_I$  and  $\sigma_{\text{pp}}^{\text{tot}}/B_R$  are connected with integrated elastic pp cross sections and thus with the rate of inelastic processes at high energies in the pp system. Our result shows that the ratio,  $\sigma_{\text{pp}}^{\text{inel}}/\sigma_{\text{pp}}^{\text{tot}} \Rightarrow \approx 2/3$  at very high energies.

To acquire a better feeling about the regularity of the energy dependence of the data and its representation by the theoretical calculation, we present in Fig. 5 results on the ratio between p-air and pp cross sections. The figure shows that this ratio has the important property of approaching a finite value for infinite energy. This information is of fundamental importance for the understanding of the geometric nature of the pp interaction and its energy dependence. The question is investigated in Sec. IV within the Glauber formalism. We show that this ratio is intimately related with the ratio  $\sigma(\text{pp inelastic})/\sigma(\text{pp total})$  and with the behaviour of the eikonal functions for large  $b$ .

The important question of the energy dependence of the ratio of p-air to pp cross sections is studied in a direct way, using properties of the  $b$  dependence of pp interaction at high energies. We show that the Yukawa-like behaviour of the interaction range, inspired in the stochastic vacuum model, explains quantitatively with high accuracy the value of the asymptotic limit of the ratio  $\sigma_{\text{p-air}}^{\text{inel}}/\sigma_{\text{pp}}^{\text{tot}}$ .

This is what we have, considering that the nucleons are the scattering centers in Glauber framework. Of course, for a ultra-high energy domain, where the pp cross section overcomes the geometric cross section of a target nucleus, the Glauber approach itself may be questionable. In the Glauber approach of pA cross section, the scattering centers inside the target are nucleons, with a fixed distribution determined by the nuclear wave function. However, at the energies where the interaction size of pp becomes large enough so that their superposition becomes not negligible, the scattering centers are rather partons and not nucleons. Then the energy dependence of pA cross section can become drastically different [23]. Here we have an open question. Further theoretical investigations of microscopic structures

leading to the asymptotic behavior in p-air cross sections will be very interesting.

### ACKNOWLEDGMENTS

The authors wish to thank the Brazilian agencies CNPq, PRONEX and FAPERJ for financial support.

- 
- [1] A. Kendi Kohara, E. Ferreira and T. Kodama , *Eur. Phys. J. C* ,**73**, 2326 (2013).
  - [2] A. K. Kohara , E. Ferreira and T. Kodama , *Phys. Rev. D* **87** , 054024 (2013).
  - [3] A. K. Kohara , E. Ferreira and T. Kodama , " *Energy Dependence and Asymptotic Behavior of pp scattering Amplitudes* ", to be published (2014).
  - [4] E. Ferreira and F. Pereira, *Phys. Rev. D* **59** , 014008 (1998) ; *Phys. Rev. D* **61**, 077507 (2000).
  - [5] H.G. Dosch, *Phys. Lett. B* **190**, 177 (1987) ; H.G. Dosch, E. Ferreira, A. Kramer *Phys. Rev. D* **50**, 1992 (1994).
  - [6] E. Ferreira, *Int. Jour. Mod. Phys. E* **16**, 2893 (2007).
  - [7] J. Beringer et al. (Particle Data Group), *Phys. Rev. D* **86**, 010001 (2012) .
  - [8] R.J. Glauber, *Phys. Rev.* 100 (1955) 242–248 ; R.J. Glauber and G. Matthiae, *Nucl. Phys. B*21(1970) 135–157.
  - [9] M. L. Good and W. D. Walker, *Phys. Rev.* 120 (1960) 1857-1860.
  - [10] R. Engel and R. Ulrich , Internal Pierre Auger Note GAP-2012, March 2012
  - [11] R. C. Barret and D. F. Jackson, *Nuclear Size and Structure*, Clarendon Oxford 1977.
  - [12] P. Abreu et al , Auger Coll., *Phys. Rev. Lett.* **109**, 062002 (2012).
  - [13] K. Belov et al. , HiRes Coll., Fly’s Eye Exp., *Nucl. Phys. B( Proc. Suppl)* **151** (2006) 197-204.
  - [14] R. M. Baltrusaitis, et al. ,Fly’s Eye Experiment , *Phys. Rev. Lett.* **52** (1984) 1380-1383.
  - [15] M. Honda , Akeno Coll., *Phys. Rev. Lett.* **70** (1993) 525-528.
  - [16] S. P. Knurenko et al. , Yakutsk Array Coll. , (1999) , Proc. of 26th ICRC (ICRC 99) (Salt Lake City, USA) Vol 1, p. 372.
  - [17] G. Aielli et al., ARGO-YBJ experiment, *Phys. Rev. D* **80**, 092004 (2009).
  - [18] H. H. Mielke et al. , *Jour. Phys. G* **20** (1994) 637 .
  - [19] M. Aglietta et al. , *Phys. Rev. D* **79**, 032004 (2009) .
  - [20] T.K. Gaisser, U.P.Sukhatme and G.B. Yodh, *Phys. Rev.D* **36** (1987) 1350-1357.
  - [21] B.Z. Kopeliovich, N.N. Nikolaev, I.K. Potashnikova *Phys. Rev. D* 39 (1989) 769.
  - [22] R. Engel, T.K. Gaisser, P. Lipari and T. Stanev, *Phys. Rev. D* **58** (1998) 014019.
  - [23] L. Portugal and T. Kodama, *Nuclear Physics A* **837** (1), 1-14 (2010).
  - [24] J. Dias de Deus, *Nucl. Phys. B* 59 (1973) 231; A.J. Buras, J. Dias de Deus, *Nucl.Phys. B* 71 (1974) 481; J. Dias de Deus, P. Kroll, *J. Phys. G* 9 (1983) L81; J. Dias de Deus, *Acta Phys. Polon. B* 6 (1975) 613.